Conformational Dynamics in Penicillin-Binding Protein 2a of Methicillin-Resistant *Staphylococcus aureus*, Allosteric Communication Network and Enablement of Catalysis

Kiran V. Mahasenan,[†] Rafael Molina,[‡] Renee Bouley,[†] María T. Batuecas,[‡] Jed F. Fisher,[†] Juan A. Hermoso,[‡] Mayland Chang,[†] and Shahriar Mobashery*,[†]

[†]Department of Chemistry and Biochemistry, University of Notre Dame, Notre Dame, Indiana 46556, United States
[‡]Department of Crystallography and Structural Biology, Institute of Physical Chemistry "Rocasolano", CSIC, 28006 Madrid, Spain

S *Supporting Information*

ABSTRACT: The mechanism of the β-lactam antibacterials is the functionally irreversible acylation of the enzymes that catalyze the cross-linking steps in the biosynthesis of their peptidoglycan cell wall. The Gram-positive pathogen *Staphylococcus aureus* uses one primary resistance mechanism. An enzyme, called penicillin-binding protein 2a (PBP2a), is brought into this biosynthetic pathway to complete the cross-linking. PBP2a effectively discriminates against the β-lactam antibiotics as potential inhibitors, and in favor of the peptidoglycan substrate. The basis for this discrimination is an allosteric site, distal from the active site, that when properly occupied concomitantly opens the gatekeeper residues within the active site and realigns the conformation of key residues to permit catalysis. We address the molecular basis of this regulation using crystallographic studies augmented by computational analyses. The crystal structures of three β-lactams (oxacillin, cefepime, ceftazidime) complexes with PBP2a—each with the β-lactam in the allosteric site—defined (with preceding PBP2a structures) as the "open" or "partially open" PBP2a states. A particular loop motion adjacent to the active site is identified as the driving force for the active-site conformational change that accompanies active-site opening. Correlation of this loop motion to effector binding at the allosteric site, in order to identify the signaling pathway, was accomplished computationally in reference to the known "closed" apo-PBP2a X-ray crystal structure state. This correlation enabled the computational simulation of the structures coinciding with initial peptidoglycan substrate binding to PBP2a, acyl enzyme formation, and acyl transfer to a second peptidoglycan substrate to attain cross-linking. These studies offer important insights into the structural bases for allosteric site-to-active site communication and for β-lactam mimicry of the peptidoglycan substrates, as foundational to the mechanistic understanding of emerging PBP2a resistance mutations.
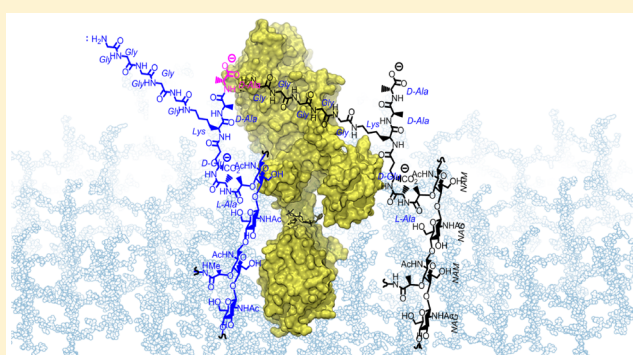
INTRODUCTION

Gram-positive infections persist as a significant cause of human morbidity and mortality, as notably exemplified by methicillin-resistant *Staphylococcus aureus* (MRSA). This bacterium is (nearly) fully resistant to all of the ensuing generations of the β-lactam class of antibiotics, as exemplified by the penicillin structure. The primary basis for MRSA resistance to the β-lactams is known.[1,2] The β-lactam antibiotics inactivate members of an essential family of enzymes, called penicillin-binding proteins (PBPs), which function in the biosynthesis of bacterial cell wall. As a result of the extensive clinical use of the β-lactams, MRSA acquired through gene transfer an additional PBP (termed PBP2a) possessing intrinsically reduced susceptibility to β-lactam inactivation. The basis for its reduced susceptibility is two-fold. The conformation of the serine nucleophile of the PBP2a active site alters to preserve reactivity toward substrate, and diminish reactivity against the β-lactam.[3] Second, the protein loop guarding the active site of PBP2a

excludes β-lactam inactivator. The conformation of the loop is regulated by an allosteric site distal (by 60 Å) from, but intimately linked to, the active site.[4,5] The endogenous ligand for the active site is the cell-wall peptidoglycan.[2] PBP2a catalyzes the cross-linking reaction between two neighboring peptidoglycan strands. A credible hypothesis is that the loop opens to substrate only when the allosteric site is occupied by a neighboring peptidoglycan. Functional evaluation of the communication between the allosteric site and active site by site-directed mutagenesis supports this assertion.[6] This hypothesis is further substantiated by the observation (also by X-ray crystallography) that ceftaroline (**1**, Figure 1A)—one of two anti-MRSA cephalosporins—binds covalently to the active site *and* non-covalently to the allosteric site.[5] Likewise, a quinazolinone ligand (**2**, Figure 1A) that binds to the allosteric
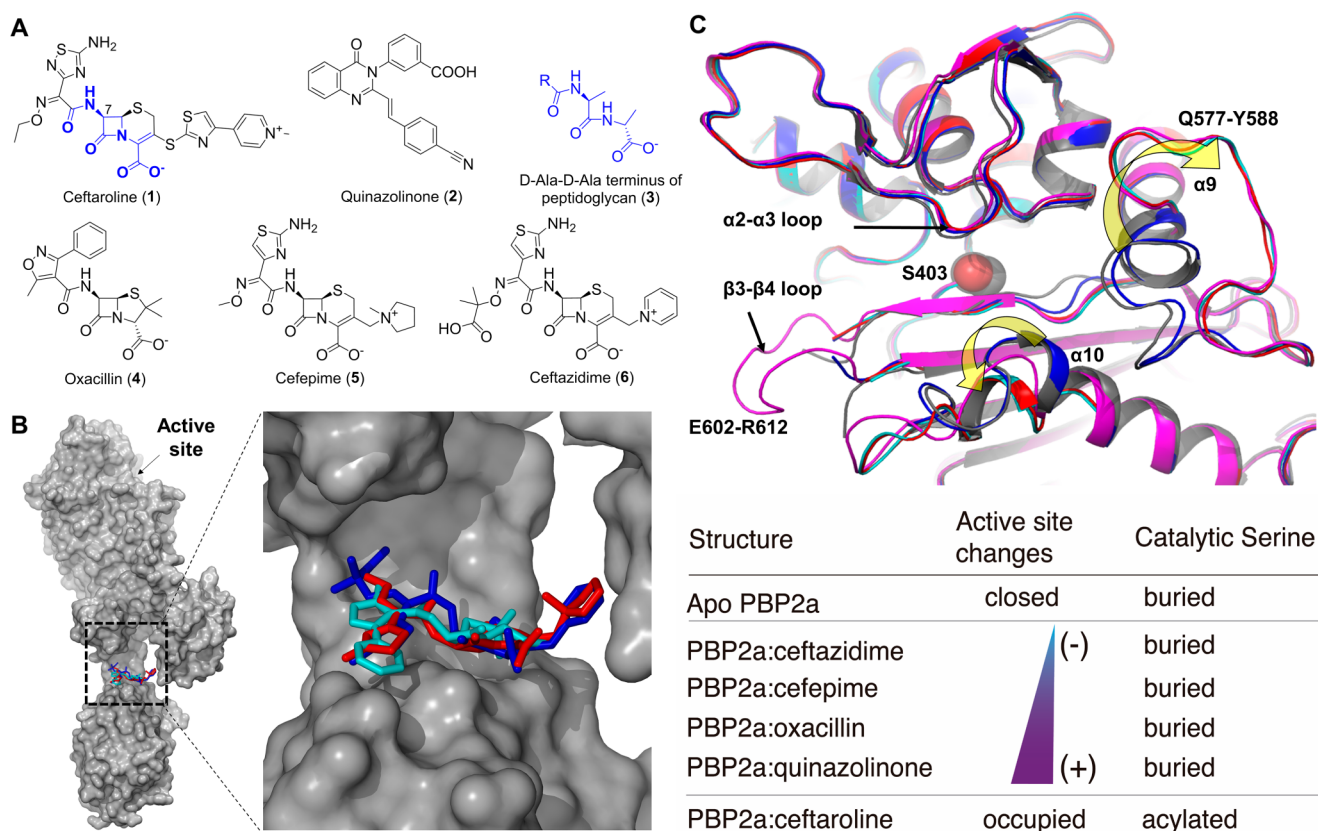
Figure 1. (A) Chemical structures of the antibacterials used in this study and the stem peptide D-Ala-D-Ala terminus. (B) Crystal structure of the PBP2a:cefepime complex showing the molecular surface (gray) and the bound cefepime as capped sticks with atoms colored in red. The structures of ceftazidime (blue capped sticks) and oxacillin (cyan capped sticks) as observed in the PBP2a:ceftazidime complex and in the PBP2a:oxacillin complex are superimposed for comparison. (C) Structural comparison of the transpeptidase domain (active site) of PBP2a in the apo structure (gray ribbon, PDB code 1VQQ), the PBP2a:ceftazidime complex (blue ribbon, this work), the PBP2a:cefepime complex (red ribbon, this work), the PBP2a:oxacillin complex (cyan ribbon, this work), and the PBP2a:quinazoline complex (magenta ribbon, PDB code 4CJN). Two translucent yellow arrows indicate the opposing directions of motion of α9 and α10 helices, which increases available space for peptidoglycan strand to approach the catalytic S403 (center, shown as sphere). The table shows the analysis of the structural changes (and the degree of it) in the transpeptidase domain of PBP2a in complex with different antibiotics compared with the apo structure. All complexes affect the active-site conformations, but to varying degrees.

site has intrinsic antibiotic activity.[7] The location of the point mutations in PBP2a that are seen in recently discovered ceftaroline-resistant clinical strains are also consistent with altered allosteric communication.[8] Allosteric regulation of the activity of PBP2a would appear to have considerable evolutionary importance. Here, we address the molecular basis of this regulation using crystallographic and computational analyses.

■ **RESULTS AND DISCUSSION**

Our objective was a unified understanding of the communication between the allosteric and active sites of PBP2a. Supported by both new and previously reported crystallographic data, we applied complementary computational approaches to this objective. We examined the conformational change that opens the active site to its first peptidoglycan substrate, which acts as the acyl donor in the cross-linking reaction. The dramatic alteration of the salt-bridge network spanning the allosteric and active sites, in response to allosteric-site occupancy, was evaluated. Correlated motions of the residues were calculated to uncover potential allosteric signaling residues. Further, the atomic details for binding of peptidoglycan substrate to the enzyme were determined, and the ensuing transacylation reaction was characterized based on a previous

quantum mechanical/molecular mechanical (QM/MM) analysis of PBP1b of *Streptococcus pneumoniae*.[9]

Substrate Access to the PBP2a Active Site. Ligand binding, whether antibiotics or peptidoglycan, at the allosteric site favors a conformational state of the protein wherein the active site is more accessible. The generality of this allosteric hypothesis was proven with several β-lactam antibiotics as mimetics of the peptide stem of the peptidoglycan.[8] The reasoning was that just as the peptidoglycan mimicry (**3**, Figure 1A) by β-lactams predisposes them for recognition at the active site,[10] the same might be true for the allosteric site.[8] Indeed, β-lactam antibiotics bind with saturation at the allosteric site.[8,11] The observation of saturation is consistent with a site that evolved for the purpose of binding an effector (here, the peptidoglycan). With the exception of ceftaroline, other β-lactam antibiotics bind only weakly. Hence, at concentrations achievable *in vivo* they cannot trigger allostery and so reverse the resistant phenotype. Notwithstanding the weak affinity of these β-lactams for the allosteric site, their ability to occupy the allosteric site was intriguing. Crystals of PBP2a were soaked with the three β-lactams (oxacillin (**4**), cefepime (**5**), and ceftazidime (**6**), Figure 1A, each with $K_d > 100 \ \mu M$ at the allosteric site[8]). All three achieved partial occupancy of the

allosteric site, with the quality of the crystals (resolution of 2.0 Å for all three, Table S1) sufficient to reveal the contour of each at the allosteric site (Figure 1B). Interestingly, none was seen in the active site: the catalytic S403 was not acylated by these β-lactams. This selectivity for the allosteric site may have resulted from the use of β-lactam structures and/or β-lactam concentrations (1−5 mM) in the crystallography experiments that are insufficient to fully activate the allosteric site and thus enable acylation of the catalytic S403 residue. We and others demonstrated previously that other β-lactams bind either exclusively to the active site (covalently)[12,13] or to both the allosteric (non-covalent) and the active sites (covalent).[5] The structures in Figure 1B show occupancy by these β-lactams only at the allosteric site, further confirming that allosteric site is the first step in the activation process of PBP2a.

Our previous X-ray analysis showed that the complex with ceftaroline at the allosteric site of PBP2a entailed notable conformational change on the β3-β4 loop in the vicinity of the active site, in comparison to the apo protein.[5] An even more pronounced conformational change was observed in the active-site region in the crystal structure of the allosteric-site-bound quinazolinone antibacterial,[7] including an unprecedented and dramatic helix-to-coil conformational change in the α9 helix (located opposite to the β3-β4 loop near the active site, Figure 1C). Notwithstanding their weak affinity for the allosteric site, all three allosteric complexes (with oxacillin, cefepime, and ceftazidime) showed—with crystallographic clarity at 2 Å resolution—strong and dramatic conformational changes at the active-site region (Figures 1C and S1). Among these changes were the restructuring of the α9 and α10 helices in the PBP2a:oxacillin and PBP2a:cefepime complexes, and the shifting of the α9 helix Q577−Y588 sequence span away from the active site (backbone root-mean-squared deviation (RMSD) of 10.1 Å for PBP2a:cefepime complex compared to apo protein). Moreover, in this PBP2a:cefepime complex the M641 residue of the α10 helix moves away (backbone RMSD change of 5.9 Å compared to apo protein) from the Y446 gatekeeper residue (as further described below). These changes adjacent to the active site improve its accessibility, and enable the approach of the second peptidoglycan (the acceptor strand) to the active site. Although the supporting residues for S403 acylation (K406, K597, S598) in all three structures show conformational progression to allow access for the approaching second peptidoglycan strand, the binding site still remains occluded for the first peptidoglycan (the donor strand used to acylate S403). Despite the observation that the β3 strand is displaced in our complexes up to 3.9 Å (at Cα of K597), the essential "twist" of the β3 strand to move G599 into contact with S403 still is not achieved (Figure S2).

The conformational change at G599/S403 occurs in response to significant conformational motion in the β3-β4 strand (residues E602−R612). A molecular dynamics (MD) simulation of the closed conformation of apo-PBP2a showed only partial β3-β4 motion, and thus only incomplete active-site opening. In contrast, the acyl-enzyme complexes derived from ceftaroline and ceftobiprole acylation of S403 acylation show the active site reorganizes following acylation. The conformational change of the protein around the C7-substituent of these cephalosporins (Figure 1A) may be visualized as identical to the change required to accommodate, in the same location, the peptide stem of the donor strand of peptidoglycan.[14,15] This conclusion is consistent with the sheltering of the active site of apo PBP2a by the α2-α3 and β3-β4 loops. Here, control of

access to the active site is most conspicuously seen in terms of the location of the side chains of the juxtaposed M641 and Y446 residues as active-site "gatekeepers". In this closed structure of the apo protein, their side chains are in direct contact, and neither antibiotic nor peptidoglycan has access to the active site.

To shed light on the mechanism used to open the active site, we chose the crystal structures of the apo and of the ceftaroline-acylated species (with the ceftaroline-derived atoms deleted; see Methods section) as two end points. A targeted molecular dynamics (TMD)[16] simulation described one plausible transition trajectory between the two structures. About 5% of the residues experienced a motion of ≥1.3 Å RMSD (Figure 2A). Among these residues, those of the β3-β4 loop were prominent (Figure 2B). Almost two-thirds of these top 5% most dynamic residues were charged. Hence, key changes in electrostatic interactions characterize the conformational changes leading to active-site opening. Although in other X-ray structures many of these 5% most dynamic residues are unresolved (indicative of their mobility), the excellent crystallographic resolution (especially of the β3-β4 loop) of the ceftaroline-acylated PBP2a gives us confidence in this interpretation. The conformational state at the end of the TMD shows full access to the active site by the stem pentapeptide. This open conformer of PBP2a enables the
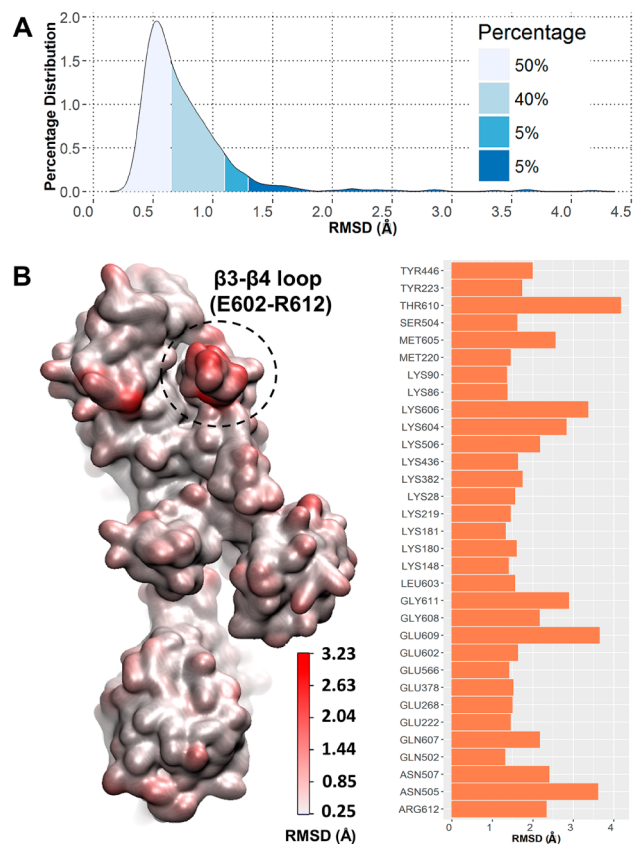

Figure 2. (A) Analysis of residue motion during the TMD simulation. (B) Left, density plot for surface residue RMSD fluctuation (red, greatest motion). RMSD values color-code the surface of the open conformation of PBP2a. The broken circle shows the location of the β3-β4 loop. Right, the identity of the top 5% dynamic residues, listed as a bar plot.

first (acyl-donor) strand of the peptidoglycan to bind en route to acylation of S403.

Salt-Bridge Interactions and Allosteric Signaling. Neither the conformations of the open and closed states, nor knowledge of the swapping of electrostatic interactions that defines the protein dynamics interconverting the two states, answers the question as to how the active and allosteric sites— separated by 60 Å—communicate. To address this question, we looked at the dynamic salt-bridge interactions along the TMD simulation trajectory of the active-site opening. All the salt-bridge pairing distances within 3.2 Å of any point in the trajectory were enumerated. A total of 125 residues (Asp, Glu, Lys, Arg, and His) participate in 79 salt-bridges (from a sampling of 1000 TMD snapshots, Figure S3). Of these, 59 fluctuate more than 3 Å during the TMD, indicating dynamic salt-bridge breakage and formation (Figure 3A). Three residues— K153, E294, and D635—each participate in three salt-bridges, highlighting intricate electrostatic connectivities. K153 and E294 are located in the allosteric site, while D635 is located between the active and allosteric sites, at a distance of 15 Å from S403. Experimental mutation of D635 (D635A) was shown previously to abolish active-site acylation, while the E294A mutation diminished acylation.[5] The TMD identified new salt-bridge interactions, which are not observed in the static crystal structures. These new salt-bridges include E150-K153 and E294-K273, both near the allosteric site. Interestingly, the E150 K mutation is observed in clinical MRSA strains resistant to ceftaroline.[17] Lastly, we analyzed the salt-bridge interactions of all of the PBP2a X-ray structures (Table S2). This analysis separates the structures into two groups, one antibiotic-acylated (open conformation) and the other apo-like (closed conformation). Several salt-bridges were present only in the acylated states, indicating a pattern for salt-bridge reformation during the conformational shift from closed to open states (Figures 3C,D and S4). Unique salt-bridges were observed at both the catalytic and allosteric sites.

Computational Identification of Allosteric "Hot-Spots" and Potential Signaling Residues. The program STRESS (STRucturally identified ESSential residues) described by Clarke et al. predicts the amino acids involved in allosteric signaling.[18] STRESS has two modules. One calculates hot-spots on the protein surface for allosteric-ligand recognition (surface-critical residues), while the second predicts buried-residue transmission (interior-critical residues). For the surface-critical residues, a series of Monte Carlo simulations of a small dummy ligand of four "atoms" linked by fixed bond length, but variable bond and dihedral angle, was performed on the surface of the protein structures, wherein the ligand probed the surface landscape with translational, rotational, and angular degrees of freedom. The attractive and repulsive energy terms accompanying contact of the ligand with the protein surface were calculated. Several thousands of such simulations on the protein structure gave the desired convergence on the predicted amino acids for allosteric binding. Further, predicted binding sites are scored based on the degree to which site distortions connect to protein motions via normal-mode analysis calculation. We evaluated 24 different PBP2a (monomer) X-ray structures with STRESS since the use of multiple X-ray structures provided a consensus, and thus greater confidence in the program's predictive power. Top-ranked five predicted binding sites in each of the 24 X-ray structures (Table S2) were ranked for the frequency of their occurrence. A total of 21 residues were identified in at least 25% of the predicted binding sites (Figures
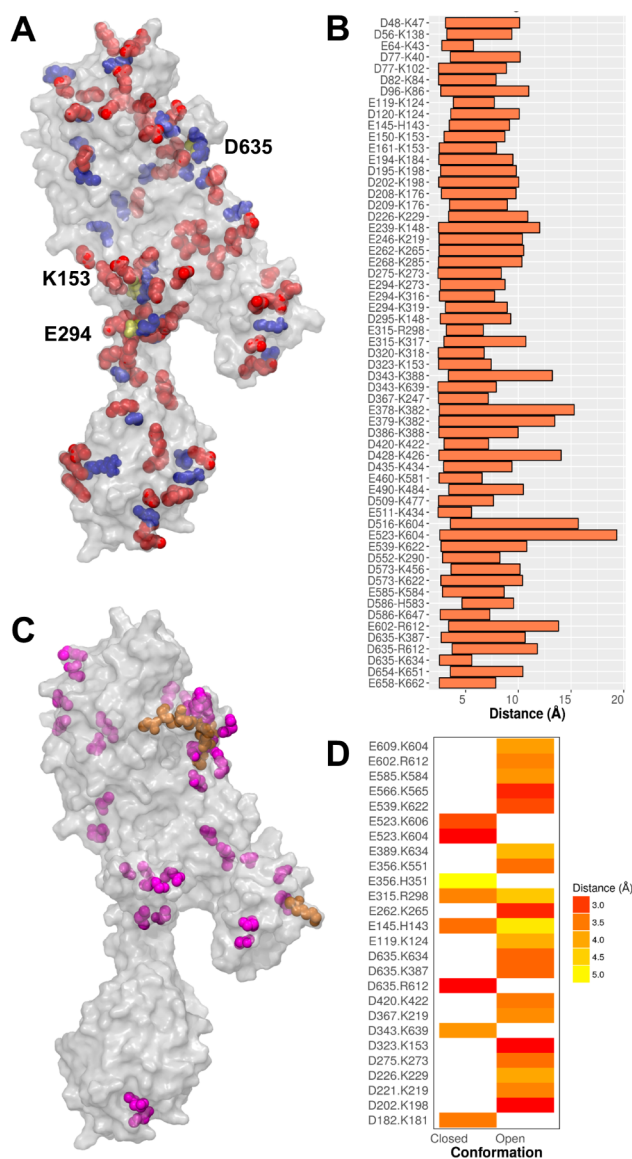

Figure 3. (A) Graphical display of the salt-bridge interactions observed during the TMD simulation, mapped on the surface (translucent) of the PBP2a apo conformation. Blue spheres (27 residues) depict residues that form salt-bridge interactions with two neighboring residues, while yellow spheres show the three interactions involving three residues (labeled). Other dynamic salt-bridge residues (≥3 Å fluctuation), which formed single salt-bridge interactions, are displayed as red spheres. (B) Cross-bar plot of the 59 most dynamic salt-bridge interactions (≥3 Å fluctuation) observed during the TMD simulation. (C) salt-bridges that are unique to each of closed (orange) and open (magenta) conformations. (D) Heatmap plot of salt-bridge distances observed from X-ray structures. (See Figure S4 for a detailed heatmap.)

4 and S5). These residues clustered in three loci. The most conspicuous cluster was located at the cleft of the allosteric site. This location of this cluster coincides precisely with the location of a peptidoglycan analogue seen by X-ray crystallography.[5] Residue D295—close to this allosteric ligand-binding cleft—was identified in 33% of the STRESS evaluations.

To predict the potential residues that propagate the response to allosteric effector binding, interior-critical residue calculations of STRESS program were performed on the same X-ray
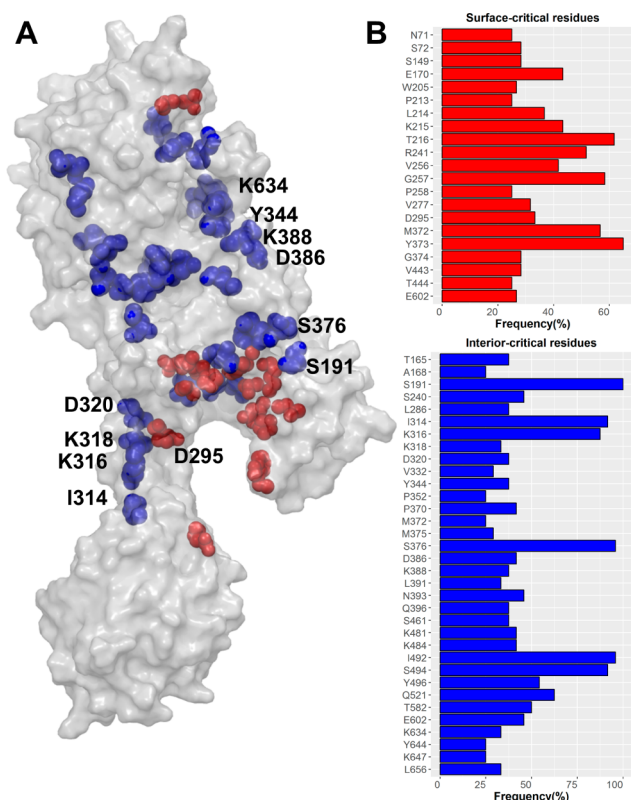
Figure 4. (A) Predicted allosteric surface-critical (red sphere representation) and interior-critical residues (blue sphere representation) mapped on the PBP2a apo conformation displayed in translucent gray surface representation. (B) Barplot of surface-critical (red) and interior-critical residues (blue) and their frequency of occurrence in the calculation performed in the study.

structures. In this method, anisotropic network model calculations identify these residues. The protein is parsed as a network of interacting residues (nodes) connected via springs (edges). Correlated and anti-correlated motions of interacting residues are calculated and weighed. This calculation detects clusters of residues, referred as "communities", which show significant connected motion within each other. A signaling path among the residue communities is inferred if a robust relationship in the motion among residues is identified. The results rank the interior residues by their frequency of occurrence. A total of 34 residues were identified in at least 25% of the structures (Figure 4). S191 and S376 were assigned as critical residues in 96% of the examples, suggesting a communication channel between the sites. I314 and K316, two of the residues in the allosteric site, were assigned as critical in 94% of the calculations. These residues and two other predicted residues (K318 and D320) are in the allosteric effector-binding site. A second residue cluster (D386, K388, Y344, K634) provides (in part) a direct interior path between the active and allosteric sites (Figure 4A). All potential residues involved in effector binding and in propagating the signal to the active site are identified (as either interior or surface paths; Figure 4B). This prediction also suggests an alternate (or supporting) interior path for allosteric site-to-active site communication.

PBP2a Catalysis of Cell-Wall Cross-Linking. The previous sections described the closed and open conformational states of PBP2a, and identified plausible structural paths for effector binding at the allosteric site to control access to the active site. Here, we describe how the two strands of peptidoglycan, one an acyl-donor substrate and the other an acyl-acceptor substrate, engage the open active site of PBP2a to fulfill its critical physiological function of cell-wall cross-linking. We had previously documented this cross-linking reaction for PBP1b of *Streptococcus pneumoniae* by QM/MM computations.[9] Our analysis here with the PBP2a structure creates an atomistic model of the catalytic cycle of PBP2a (Figure S6), which merges seamlessly with the aforementioned QM/MM model. The details of the catalytic events for PBP1b and PBP2a are similar. The difference is that the latter is regulated by allostery, whereas the former is not.

We used the open conformation of ceftaroline-acylated PBP2a structure (PDB code 3ZG0) to model the complex with the first peptidoglycan strand and its subsequent acylation of S403. The ceftaroline atoms were computationally removed and the system was energy-minimized. The catalytic Lys406 was assigned as the free base. An eight-saccharide long peptidoglycan segment (Figure 5) was used for both substrates (PG1, acyl donor; PG2, acyl acceptor). The solution conformation of the peptidoglycan strand was used to model both PG1 and PG2 segments.[19] The PG1 segment was docked into the active site and scored using the GLIDE program (v 6.7, Schrödinger LLC, New York)[20] enforcing a 1 Å core restraint for the acyl-D-Ala-D-Ala stem-peptide terminus to match the β-lactam core, which it mimics (Figure 1A). The high-scored poses were nearly identical to the Michaelis complex for the *S. pneumoniae* PBP1b-peptidoglycan complex calculated by QM/MM (Figure S7).[9] A representative pose was selected for MD simulation (see Methods section). The structure, corresponding to the pre-acylation complex of PBP2a with PG1, was solvated in a rectangular box of TIP3P water molecules and neutralized by the addition of Na⁺ ions. The system was energy minimized with the PMEMD module of the AMBER 14 suite,[16] followed by MD simulation for 1 ns to evaluate the substrate–enzyme interaction. Charges for the peptidoglycan strand were calculated by the RESP method at HF/6-31G(d) level of QM theory.[21] AMBER ff12SB and General AMBER force field provided the MM parameters for the system.

The key substrate–enzyme interactions in the resulting computational structure are summarized. The peptide stem occupies a narrow cleft formed by the β3-β4 loop within the active site (Figure S7). The *S. aureus* Gly₅ extension on the lysine sits in a depression flanked by E602, M641, and Y446. In this orientation, the pentaglycyl moiety is exposed to solvent. The backbone carbonyl oxygen of the PG1 Lys forms a hydrogen bond with the highly conserved N464, suggesting a role in substrate positioning within the catalytic site. The D-Ala-D-Ala segment occupies the active site so as to nicely position the methyl of the penultimate D-Ala into a small pocket lined by Y519. Position 519 in other PBPs is conserved as a tyrosine or other hydrophobic residue (F/I/L/M), suitable for binding to the methyl group. The carbonyl oxygen of this D-Ala is ensconced in the "oxyanion hole" formed by hydrogen bonds with the backbone amides of T600 and S403 (Figure 5A, species I). The carboxylate functionality of the terminal D-Ala occupies the same position as the C4-carboxylate of ceftaroline as seen from its X-ray structure, and forms a hydrogen bond with S462. Guided by the QM/MM study of PBP1b,[9] we used the MM method to model the three ensuing structures in turnover. To model the covalent acyl-enzyme intermediate, the terminal D-Ala (the leaving group) was removed and a bond created to interconnect the penultimate D-Ala to the catalytic S403. This acyl enzyme was solvated, energy-minimized, and
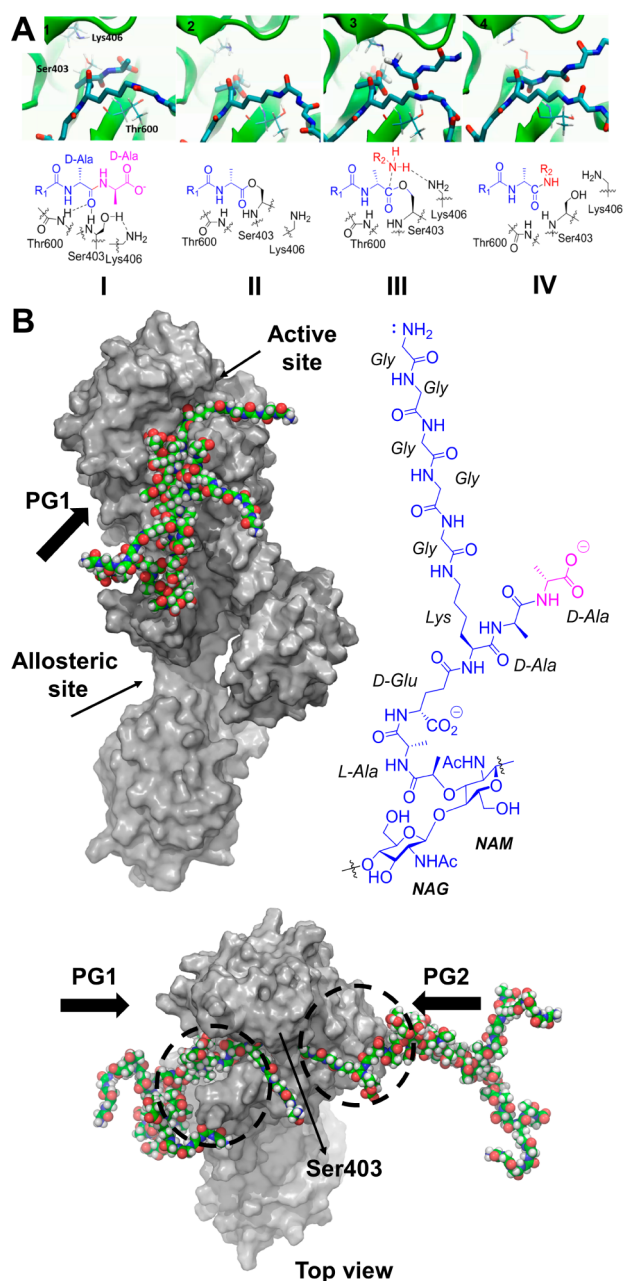
Figure 5. (A) Modeled species along the catalytic reaction of PBP2a, based on the QM/MM calculations. The species are (I) the preacylation complex with the first peptidoglycan strand (PG1, blue and pink chemical structure); (II) the acylated S403 species (by PG1); (III) the approach of the second peptidoglycan strand in the deacylation complex (PG2, depicted in red in the chemical structure); (IV) the cross-linked PG1-PG2 product in the catalytic pocket. (B) Model of the first peptidoglycan strand (an octasaccharide strand, CPK representation, colored by atom type) bound to the open active site of PBP2a representing the preacylation complex (surface representation). A view down the axis of the protein from 12 o'clock is shown at the bottom for the enzyme–product (cross-linked peptidoglycan) complex. This perspective shows the meeting of the two strands of the peptidoglycan (PG1 and PG2) within the active site. The regions of conformational change in PBP2a are highlighted with the broken circles. Right, the structure of a disaccharide NAG-NAM with the Gly$_5$ stem extension seen for *S. aureus*.

subjected to MD simulation following the same protocol as described above. The resulting structure (species II) shows high

similarity to the structure of S403 acylated by ceftaroline (Figure S7). Both species I and II show two hydrogen bonds to T600. The ethoxyimino group of ceftaroline occupies the same position and orientation as the lysine of the peptide stem, suggesting yet additional mimicry between the ceftaroline and peptidoglycan structures. The departure of the D-Ala leaving group opens access to the acyl enzyme from the opposite side of the active site. The aforementioned conformational changes of the α9 and α10 helices facilitate this access. To model peptidoglycan cross-linking, a molecular docking protocol was used to bring the terminal amine of the pentaglycyl moiety of the second peptidoglycan strand (PG2) into close proximity to the carbonyl of the acyl enzyme. The resulting complex (species III) was solvated and simulated by MD. The highly conserved T600 residue forms a hydrogen bond with the carbonyl oxygen of the terminal glycine, and positions the amine for acyl transfer to complete the cross-linking. The cross-linked product (species IV) was modeled into the active site and subjected to MD simulation.

Turnover of the PBP2a catalytic cycle is stepwise. Opening one side of the active site is essential to allow entry of the first peptidoglycan strand for acylation of the active-site S403 (Figure 5B). The TMD simulation we described in the previous section demonstrates this first conformational reorganization at the active site. Subsequent opening of the active site on the other side, exemplified by the crystal structures of PBP2a with allosteric-site bound β-lactams, allows entry of the second strand of peptidoglycan. Acyl transfer liberates S403 and gives cross-linked peptidoglycan as product. Remarkably, this mechanism ingeniously serves the key purpose of shielding the active site of PBP2a. On the other hand, it may be worth to note that *S. pneumoniae* PBP1b active site is natively unsheltered (Figure S7).

Conclusion: The Allosteric PBP2a Catalyst. The perspectives shown in Figure 5 highlight the structural breadth of the bifurcated cross-protein channels used by PBP2a to position its two peptidoglycan substrates for cross-linking, and their spatial relationship to the allosteric site. These static perspectives do not offer answers to two fundamental questions concerning PBP2a catalysis: the functional integration of the allosteric site with the active site, and the atomistic-level structural basis that drives the communication between these sites. Answers to both questions are necessarily rudimentary at this stage.

Knowledge of the spatial pattern for the cross-linking as shown in Figure 5, and the fact that the endogenous effector for the allosteric site is the peptidoglycan itself, in principle sets limits on the three-dimensional structure of the peptidoglycan polymer. The unknown structure of this polymer—arguably the last grand biological polymer with unknown structure—is a continuing topic of interpretation and uncertainty. Accordingly, consideration of how the allosteric site integrates with catalysis must be made apart from consideration of the conformational character of either the assembling peptidoglycan, or of the final peptidoglycan product. We can however offer a mechanistic concept. A putative multi-protein complex (including PBP2a) that assembles the cell wall must translocate. Accepting the long-standing hypothesis that peptidoglycan synthesis uses existing peptidoglycan as a template,[22,23] one can conceptualize peptidoglycan synthesis as occurring by steps from an in-register state (with respect to catalysis), followed by motion coinciding with an out-of-register state, and return to an in-register state for the next turnover. This concept visualizes

alternate effector occupancy of (and release from) the allosteric site, coinciding directly with alternate opening (and closing) of the active site. The value of the allosteric site to PBP2a is that the active site is closed, and therefore protected from β-lactam inactivation, during all out-of-register motions. When PBP2a encounters an exceptionally efficacious β-lactam structure (as a result of exceptional mimicry of the stem peptide), its occupancy of the allosteric site leaves PBP2a in a perpetually vulnerable open state, and as well conceivably preventing PBP2a from attaining the proper registry for its next turnover. This would appear to be the case with ceftaroline.

An important corollary to this concept of PBP2a catalysis occurring through alternate effector occupancy (coinciding with only periodic active-site opening) is that the open and closed PBP2a states must be equivalent in energy, and interchanged with small activation energy. As understanding protein conformational dynamics (such as exemplified by intrinsically disordered proteins)[24] where the energy states are unequal and the activation barrier are greater is itself a profound challenge, the search for an atomistic-level structural "trigger" interconnecting effector binding with active-site opening, is arguably futile. Rather, the focus has to remain—in terms of both β-lactam antibiotic design and allosteric site occupancy—on the ability of the β-lactam to attain effective mimicry of the peptidoglycan stem. An important means of assessing the structural basis of effective mimicry is through interpretation of resistance mutations, several of which are now known for PBP2a (notably, including the allosteric site).[25−27] The analysis of PBP2a mutants, using the methodology that we describe here, may provide useful insight into the relationship between effective β-lactam mimicry and PBP2a structure.

Notwithstanding the usefulness of such insight, the challenge of antimicrobial resistance cannot be reduced to overcoming a pairwise correlation. Resistance is always the result of incremental benefit realized across multi-factorial adaptation. MRSA is a profound teaching example of this reality. Optimal efficacy of new β-lactams against *S. aureus* will require consideration not just of PBP2a but also of a second PBP (PBP4) of this bacterium.[28−30] This objective too sets future crystallographic and computational opportunities.

■ METHODS

Crystallization. Wild-type PBP2a crystals were grown following the procedure previously described.[5] Wild-type PBP2a crystals were soaked in the precipitation solution containing 5 mM oxacillin, 1 mM ceftazidime, or 1 mM cefapime for 24 h at 4 °C, respectively. Crystals were then soaked briefly in a cryo-protectant solution (0.1 M HEPES pH 7, 28% PEG 550 MME, 1 M NaCl, 16 mM CdCl₂) prior to flash cooling at 100 K.

Data Collection, Structure Solution, Model Building, and Refinement. All data were collected from frozen crystals at 100 K with PILATUS detectors at beamlines PXI (SLS, Villigen, Switzerland) and XALOC (ALBA Synchrotron, Barcelona, Spain). Data processing and scaling were accomplished with XDS[31] and Scala from the CCP4 package.[32] Statistics for the crystallographic data and structure solution are summarized in Table S1. The structures were solved by molecular replacement, as implemented in the program PHASER.[33] The search models were based on the PDB entry 1VQQ corresponding to the apo PBP2a. Two monomers (chains A and B) were present in the asymmetric units of each of the three complexes. The models were then subjected to iterative cycles of model building and refinement with Coot[34] and PHENIX.[35] All three complexes were solved at high resolution (1.98–2.00 Å) (Table S1). The electron-density maps showed important changes in the backbone of the protein at the active sites of the transpeptidase domains of monomers B for the three

antibiotics. No electron density was, however, observed at the active sites and the catalytic S403 remained in an unacylated form. Electron density was observed at the allosteric site of the same monomers, which also experienced changes within the respective active sites. Significance of the electron density at allosteric sites was further confirmed by calculation of unbiased omit maps (Polder Maps) in PHENIX. Inclusion of the antibiotics in the refinement provided the final electron-density maps that exhibited poor occupancy due to poor affinity.

As also reported in previous PBP2a complexes (PDB codes 3ZG0 and 4CJN), a muramic acid molecule was found at the allosteric site in all three complexes, revealing the muropeptide location observed in the PBP2a:muropetide complex (PDB code 3ZG5). The electron-density maps for the muramic acid are remarkably good in all PBP2a complexes. Ramachandran statistics for PBP2a:oxacillin complex showed that 96.77% residues were in most favored regions, 2.68% residues in allowed regions, and 0.55% in disallowed regions. For PBP2a:cefepime, 95.30% residues were in most favored regions, 3.68% residues in allowed regions, and 1.02% in disallowed regions, while for PBP2a:ceftazidime complex, 96.00% residues were in most favored regions, 3.45% residues in allowed regions, and 0.55% in disallowed regions. The corresponding coordinates and structure factors are deposited in the protein data bank as 5M19, 5M18, and 5M1A for PBP2a:oxacillin, PBP2a:cefepime and PBP2a:ceftazidime, respectively.

Targeted Molecular Dynamics (TMD) Simulation of Active-Site Opening. TMD was performed with sander module of AMBER 14 suite applying AMBER ff12SB forcefiled.[16] In the TMD simulation, atoms in initial closed conformation was guided toward final "target" open structure by applying a steering force based on a mass-weighted RMSD with respect to reference target conformation. The closed [apo conformation, PDB code 1MWR] and open [ceftaroline acylated conformation, PDB code 3ZG0] crystal structures were prepared for molecular-dynamics simulation using Maestro program (v 2015, Schrödinger, LLC, New York). The amino-acid residues from D27 to E668 were retained in the structures used for the simulation. The selenomethionine residues in the apo conformation were mutated to methionine. Ceftaroline and muramic-acid atoms were removed from the open conformation. Protonation states for histidines were assigned and hydrogen atoms were added, followed by a constrained energy minimization with OPLS2005 force field. Leap module of AMBER 14 was used to solvate the structures centered on a rectangular box of TIP3P water model with edges at least 15 Å away from the protein surface. PMEMD module was used to minimize the energy of the system in three successive stages each of 500 steps of steepest descent, followed by 2000 steps of conjugate-gradient method. During the first stage, hydrogen atoms were energy-minimized while restraining the rest of the atoms. In the subsequent stage, water molecules were energy-minimized. Finally, the entire system was energy-minimized without any restraints. The system was then equilibrated in five stages starting with a heating stage in which the temperature was raised gradually from 0 to 300 K over 50 ps in NVT ensemble. Subsequent stages of the simulation were performed in NPT ensemble (constant pressure and temperature of 1 atm and 300 K, respectively). The second stage of equilibration (50 ps) allowed water molecules to equilibrate while restraining the protein in order to sufficiently solvate the protein surface. The ensuing 300 ps equilibration involved gradual release of the restraints on the protein residues. The final equilibrated system coordinates were used for the TMD simulation. TMD was carried out such that the closed conformation reaches the open conformation over 1 ns of simulation time. A weak force constant of 0.1 kcal/(mol·Å²) was applied for the targeted simulation with linearly decrementing target RMSD value to zero. Berendsen barostat and thermostat were employed for pressure and temperature controls, respectively.[36] Bonds to hydrogen atoms were constrained with SHAKE algorithm allowing a time step of 2 fs for the simulations.[37] Periodic boundary condition was applied with a cutoff value of 8 Å for nonbonded interactions. Longer-range electrostatics was simulated by Particle Mesh Ewald method.[38] Trajectory was collected for each picosecond of the simulation resulting in 1000 snapshots.

Enumeration and Distance Calculation of Salt-Bridges in PBP2a. Salt-bridge interactions were analyzed with Salt-Bridges Plugin, v1.1 implemented in VMD program (v 1.9.2).[39,40] A salt-bridge is considered to be formed if the oxygen atoms of acidic residues were within the cutoff distance of 3.2 Å from the nitrogen atoms of basic residues in at least one snapshot among the sampled 1000 TMD simulation snapshots. For the enumerated salt-bridges, the salt-bridge distances were measured between the center of mass of the oxygens in the acidic side chain and center of the mass of the nitrogen atoms in the basic side chain.

Salt-Bridge Analysis of PBP2a Crystal Structures. Available X-ray structures were downloaded from the Protein Data Bank (www.rcsb.org). The monomer chains from each dimers were separated and superimposed to generate a structural alignment of all the conformations. The acylated monomers were observed to be in an open conformation (for the approach of PG1), while the apo structures showed closed conformation at the active site. Based on this observation, the structures were grouped into open and closed conformations (Table S2). The missing loops in the monomers were modeled based on other X-ray structures within their same group. Salt-bridge interactions were enumerated for all the chains employing the method described above. Unique salt-bridges for the closed and open conformations were identified from the data set and plotted using ggplot2 module of the R program.

Allosteric-Critical Residue Prediction by STRESS Program. The STRESS program was downloaded from the online server and installed on a local Linux workstation.[18] All the calculations were performed locally. The previously prepared 24 PBP2a X-ray structure monomer chains, as listed in the Table S2, were used for the calculation of surface-critical and interior-critical residues.

PBP2a-Peptidoglycan Complex Modeling and Simulation. The open ceftaroline acylated crystal structure (PDB code 3ZG0) was prepared using Maestro program, as described in the TMD simulation section. A capped D-Ala-D-Ala dipeptide was modeled on the active site based on the ceftaroline atom locations in order to restrain the ensuing docking calculations. The peptide stem of peptidoglycan was docked to the active site using the GLIDE program[20] enforcing restraints for the D-Ala-D-Ala atomic coordinates. The top-scored docked solutions were compared with previous QM/MM Michaelis complex for the *S. pneumoniae* PBP1b-peptidoglycan complex.[9] This docked coordinate provided template structure to model the rest of the octasaccharide peptidoglycan segment. The complete octasaccharide segment of the peptidoglycan was modeled based on the reported NMR solution structure.[19] This coordinate was superimposed to the docked D-Ala-D-Ala segment and the rest of the region was manually modeled based on the QM/MM Michaelis complex for the *S. pneumoniae* PBP1b-peptidoglycan complex.[9] The model was subsequently energy minimized with IMPACT program (Schrödinger LLC, New York, 2015) employing OPLS2005 force field. The final coordinate from the docking calculation was subjected to molecular-dynamics simulation with AMBER 14 package. Explicit water solvation, energy minimization, and equilibration simulation were performed as described above for TMD simulation. Subsequent production simulations, in the NPT ensemble, were carried out for 1 ns with PMEMD module.

ASSOCIATED CONTENT

Ⓢ Supporting Information

The Supporting Information is available free of charge on the ACS Publications website at DOI: 10.1021/jacs.6b12565.

> Methods of computational analysis, X-ray crystallography, and other details, including Tables S1 and S2 and Figures S1–S7 (PDF)
> Movie (AVI)

AUTHOR INFORMATION

Corresponding Author
*mobashery@nd.edu

ORCID Ⓘ
Shahriar Mobashery: 0000-0002-7695-7883

Notes
The authors declare no competing financial interest.

REFERENCES

(1) Dordel, J.; Kim, C.; Chung, M.; Pardos de la Gandara, M.; Holden, M. T.; Parkhill, J.; de Lencastre, H.; Bentley, S. D.; Tomasz, A. *mBio* **2014**, *5*, e01000-13.

(2) Peacock, S. J.; Paterson, G. K. *Annu. Rev. Biochem.* **2015**, *84*, 577.

(3) Lovering, A. L.; Safadi, S. S.; Strynadka, N. C. *Annu. Rev. Biochem.* **2012**, *81*, 451.

(4) Fuda, C.; Hesek, D.; Lee, M.; Morio, K.; Nowak, T.; Mobashery, S. *J. Am. Chem. Soc.* **2005**, *127*, 2056.

(5) Otero, L. H.; Rojas-Altuve, A.; Llarrull, L. I.; Carrasco-Lopez, C.; Kumarasiri, M.; Lastochkin, E.; Fishovitz, J.; Dawley, M.; Hesek, D.; Lee, M.; Johnson, J. W.; Fisher, J. F.; Chang, M.; Mobashery, S.; Hermoso, J. A. *Proc. Natl. Acad. Sci. U. S. A.* **2013**, *110*, 16808.

(6) Fishovitz, J.; Rojas-Altuve, A.; Otero, L. H.; Dawley, M.; Carrasco-Lopez, C.; Chang, M.; Hermoso, J. A.; Mobashery, S. *J. Am. Chem. Soc.* **2014**, *136*, 9814.

(7) Bouley, R.; Kumarasiri, M.; Peng, Z.; Otero, L. H.; Song, W.; Suckow, M. A.; Schroeder, V. A.; Wolter, W. R.; Lastochkin, E.; Antunes, N. T.; Pi, H.; Vakulenko, S.; Hermoso, J. A.; Chang, M.; Mobashery, S. *J. Am. Chem. Soc.* **2015**, *137*, 1738.

(8) Fishovitz, J.; Taghizadeh, N.; Fisher, J. F.; Chang, M.; Mobashery, S. *J. Am. Chem. Soc.* **2015**, *137*, 6500.

(9) Shi, Q.; Meroueh, S. O.; Fisher, J. F.; Mobashery, S. *J. Am. Chem. Soc.* **2011**, *133*, 5274.

(10) Tipper, D. J.; Strominger, J. L. *Proc. Natl. Acad. Sci. U. S. A.* **1965**, *54*, 1133.

(11) Villegas-Estrada, A.; Lee, M.; Hesek, D.; Vakulenko, S. B.; Mobashery, S. *J. Am. Chem. Soc.* **2008**, *130*, 9212.

(12) Lim, D.; Strynadka, N. C. *Nat. Struct. Biol.* **2002**, *9*, 870.

(13) Lovering, A. L.; Gretes, M. C.; Safadi, S. S.; Danel, F.; de Castro, L.; Page, M. G.; Strynadka, N. C. *J. Biol. Chem.* **2012**, *287*, 32096.

(14) Lee, M.; Hesek, D.; Suvorov, M.; Lee, W.; Vakulenko, S.; Mobashery, S. *J. Am. Chem. Soc.* **2003**, *125*, 16322.

(15) Lee, W.; McDonough, M. A.; Kotra, L.; Li, Z. H.; Silvaggi, N. R.; Takeda, Y.; Kelly, J. A.; Mobashery, S. *Proc. Natl. Acad. Sci. U. S. A.* **2001**, *98*, 1427.

(16) Case, D. A.; et al. *AMBER*; University of California, San Francisco, 2014.

(17) Mendes, R. E.; Tsakris, A.; Sader, H. S.; Jones, R. N.; Biek, D.; McGhee, P.; Appelbaum, P. C.; Kosowska-Shick, K. *J. Antimicrob. Chemother.* **2012**, *67*, 1321.

(18) Clarke, D.; Sethi, A.; Li, S.; Kumar, S.; Chang, R. W.; Chen, J.; Gerstein, M. *Structure* **2016**, *24*, 826.

(19) Meroueh, S. O.; Bencze, K. Z.; Hesek, D.; Lee, M.; Fisher, J. F.; Stemmler, T. L.; Mobashery, S. *Proc. Natl. Acad. Sci. U. S. A.* **2006**, *103*, 4404.

(20) Friesner, R. A.; Banks, J. L.; Murphy, R. B.; Halgren, T. A.; Klicic, J. J.; Mainz, D. T.; Repasky, M. P.; Knoll, E. H.; Shelley, M.; Perry, J. K.; Shaw, D. E.; Francis, P.; Shenkin, P. S. *J. Med. Chem.* **2004**, *47*, 1739.

(21) Cornell, W. D.; Cieplak, P.; Bayly, C. I.; Kollmann, P. A. *J. Am. Chem. Soc.* **1993**, *115*, 9620.

(22) Holtje, J. V. *Microbiol. Mol. Biol. Rev.* **1998**, *62*, 181.

(23) Vollmer, W.; Bertsche, U. *Biochim. Biophys. Acta, Biomembr.* **2008**, *1778*, 1714.

(24) Oldfield, C. J.; Dunker, A. K. *Annu. Rev. Biochem.* **2014**, *83*, 553.

(25) Alm, R. A.; McLaughlin, R. E.; Kos, V. N.; Sader, H. S.; Iaconis, J. P.; Lahiri, S. D. *J. Antimicrob. Chemother.* **2014**, *69*, 2065.

(26) Long, S. W.; Olsen, R. J.; Mehta, S. C.; Palzkill, T.; Cernoch, P. L.; Perez, K. K.; Musick, W. L.; Rosato, A. E.; Musser, J. M. *Antimicrob. Agents Chemother.* **2014**, *58*, 6668.

(27) Lahiri, S. D.; Alm, R. A. *J. Antimicrob. Chemother.* **2016**, *71*, 34.

(28) Qiao, Y.; Lebar, M. D.; Schirner, K.; Schaefer, K.; Tsukamoto, H.; Kahne, D.; Walker, S. *J. Am. Chem. Soc.* **2014**, *136*, 14678.

(29) Chan, L. C.; Gilbert, A.; Basuino, L.; da Costa, T. M.; Hamilton, S. M.; Dos Santos, K. R.; Chambers, H. F.; Chatterjee, S. S. *Antimicrob. Agents Chemother.* **2016**, *60*, 3934.

(30) Lahiri, S. D.; Alm, R. A. *J. Antimicrob. Chemother.* **2016**, *71*, 3050.

(31) Kabsch, W. *Acta Crystallogr., Sect. D: Biol. Crystallogr.* **2010**, *66*, 125.

(32) Evans, P. *Acta Crystallogr., Sect. D: Biol. Crystallogr.* **2006**, *62*, 72.

(33) McCoy, A. J.; Grosse-Kunstleve, R. W.; Adams, P. D.; Winn, M. D.; Storoni, L. C.; Read, R. J. *J. Appl. Crystallogr.* **2007**, *40*, 658.

(34) Emsley, P.; Lohkamp, B.; Scott, W. G.; Cowtan, K. *Acta Crystallogr., Sect. D: Biol. Crystallogr.* **2010**, *66*, 486.

(35) Adams, P. D.; Afonine, P. V.; Bunkoczi, G.; Chen, V. B.; Davis, I. W.; Echols, N.; Headd, J. J.; Hung, L. W.; Kapral, G. J.; Grosse-Kunstleve, R. W.; McCoy, A. J.; Moriarty, N. W.; Oeffner, R.; Read, R. J.; Richardson, D. C.; Richardson, J. S.; Terwilliger, T. C.; Zwart, P. H. *Acta Crystallogr., Sect. D: Biol. Crystallogr.* **2010**, *66*, 213.

(36) Berendsen, H. J. C.; Postma, J. P. M.; Vangunsteren, W. F.; Dinola, A.; Haak, J. R. *J. Chem. Phys.* **1984**, *81*, 3684.

(37) Ryckaert, J. P.; Ciccotti, G.; Berendsen, H. J. C. *J. Comput. Phys.* **1977**, *23*, 327.

(38) Darden, T.; York, D.; Pedersen, L. *J. Chem. Phys.* **1993**, *98*, 10089.

(39) Knapp, B.; Lederer, N.; Omasits, U.; Schreiner, W. *J. Comput. Chem.* **2010**, *31*, 2868.

(40) Humphrey, W.; Dalke, A.; Schulten, K. *J. Mol. Graphics* **1996**, *14*, 33.